agriculture

Article

A Fault Diagnosis Method for a Differential Inverse Gearbox of a Crawler Combine Harvester Based on Order Analysis

Yaoming Li *, Yanbin Liu, Kuizhou Ji and Ruiheng Zhu

Key Laboratory of Modern Agricultural Equipment and Technology, Ministry of Education, Jiangsu University, Zhenjiang 212013, China
* Correspondence: ymli@ujs.edu.cn

Abstract: The single HST (Hydro Static Transmission) mechanical differential transmission gearbox of crawler combine harvester is subjected to the impact of alternating loads in the field operation, resulting in its fatigue failure. The traditional durability fatigue test can improve the fault-free working time of machinery, but it is not suitable for agricultural machinery with time-varying load frequency bandwidth and stress amplitude. Therefore, in this paper, a fault diagnosis method based on order analysis was proposed considering the comprehensive influence of load amplitude and frequency on the fatigue life of gearbox. The location and the corresponding type of fault were found by comparing the spectral line peak changed before and after. Then, the test verification was carried out on the gearbox assembly fatigue test bench according to the compiled load spectrum. The results show that the analysis results of the fault diagnosis method based on order analysis were consistent with the unpacking inspection, which had reference significance for the research on the fault diagnosis method of the crawler combined harvester gearbox.

Keywords: combine harvester; differential inverse gearbox; order analysis; fault diagnosis method; fatigue test

check for updates

Citation: Li, Y.; Liu, Y.; Ji, K.; Zhu, R. A Fault Diagnosis Method for a Differential Inverse Gearbox of a Crawler Combine Harvester Based on Order Analysis. *Agriculture* **2022**, *12*, 1300. https://doi.org/10.3390/agriculture12091300

Academic Editors: Muhammad Sultan, Redmond R. Shamshiri, Md Shamim Ahamed and Muhammad Farooq

Received: 27 July 2022
Accepted: 22 August 2022
Published: 25 August 2022

Publisher's Note: MDPI stays neutral with regard to jurisdictional claims in published maps and institutional affiliations.

Copyright: © 2022 by the authors. Licensee MDPI, Basel, Switzerland. This article is an open access article distributed under the terms and conditions of the Creative Commons Attribution (CC BY) license (https://creativecommons.org/licenses/by/4.0/).

1. Introduction

The single HST (hydro static transmission) mechanical differential inverse gearbox is one of the important parts of the transmission system of a crawler combine harvester; it can realize radius steering, unilateral braking steering and differential steering. Due to the harsh working environment of combine harvester, the gearbox bears complex alternating loads for a long time in the working process [1]. Therefore, the gearbox is prone to fatigue failure, which seriously affects the fault-free working time of the machinery [2–4]. To improve the service life of the gearbox, the tester generally judge faults in the gearbox through traditional durability fatigue tests based on its abnormal running conditions [5]. However, this method cannot determine the initial location and type of early faults when various faults occur in the gearbox. Therefore, gearbox fault diagnosis is a very important topic in the field of machinery diagnostics.

The fault vibration signal in the early stage of gearbox is weak and difficult to be detected under the interference of noise or other signals. However, when the external driving speed and load change, the early fault information hidden during the stable working condition may be highlighted [6]. In this case, the frequency components of vibration signals under non-stationary conditions are complex, and the characteristic parameters of fault signals are time-varying. The natural frequency and damping ratio of the impact response components representing local faults will fluctuate under the influence of variable loads, and the impact response interval is no longer periodic. Traditional spectrum analysis technology is prone to 'frequency ambiguity' phenomenon, resulting in missed diagnosis and misjudgment [7].

Therefore, many fault diagnosis methods for non-stationary vibration signals have been proposed, for instance, time-frequency analysis and order analysis [8]. Order analysis is one of the effective methods for the non-stationary signal analysis of rotating machinery, and its main idea is to map time-varying frequency components into constant frequency components [9]. In recent years, the fault diagnosis technology of gearboxes based on order analysis has been receiving increasing attention. Wan et al. [10] proposed a time-domain synchronous averaging method based on order analysis for the offline detection of an automobile gearbox. By intercepting several signal segments equal to the specified periodic signal and averaging them, the periodic signal can be separated from the random signal, which was helpful for the rapid fault diagnosis of the downline. Feng et al. [9] studied the fault diagnosis of a planetary gearbox under non-stationary conditions based on the combined envelope and frequency order spectrum analysis of iterative generalized demodulation. Through the comparative analysis of planetary gearbox simulation and engineering tests, the authors verified that the proposed method could effectively extract distributed and local gear faults under non-stationary conditions. He et al. [11] proposed a novel order tracking method to analyze the fault diagnosis of wind turbine gearbox based on discrete spectrum correction technique. The effectiveness and robustness of the proposed method were verified through simulations and actual tests. However, the order analysis method has not been reported in the field of fault diagnosis of single HST (hydro static transmission) mechanical differential inverse gearbox for crawler combine harvester.

Therefore, in this paper, a gearbox fault diagnosis method for crawler combine harvester based on order analysis was proposed. The detailed objectives were: (1) to simulate the main working conditions of differential inverse gearbox in the room, its fatigue test bench was built; (2) to establish the order calculation model of differential reverse gearbox to obtain the main meshing order of gears and the first harmonic of key bearing order in common working gear; (3) to carry out the experimental verification on the gearbox assembly fatigue test bench according to the compiled load spectrum.

2. Materials and Methods

2.1. Structure and Working Principle of Differential Inverse Gearbox

The structure of the mechanical differential inverse gearbox is shown in Figure 1 [12,13]. When the harvester moved forward, the engine transmitted its driving force to the HST via belts and pulleys. Then, when the tooth was embedded in the structure on the left and right sides, the power was transmitted to the output half shaft on both sides through the first stage gear transmission (1, 2), the second stage gear transmission (3, 4, 5, 6), the third stage gear transmission (7, 9), the fourth stage gear transmission (10, 12) and the fifth stage gear transmission (12, 13). This caused the drive wheels on both sides of the chassis to output equivalent rotational speed in the same direction. When the harvester turned left, the left tooth embedded structure was separated, and the power output on the right was normal. The walking chassis realized unilateral braking steering by locking the unilateral brake gear to the clutch driven gear (10), and the steering radius was about half of the track center distance. When the central gear ring of the clutch driving gear (8) was locked by the differential steering brake gear (11), the power on the right side was transferred to the left side through the planetary gear meshing transmission to reverse the differential steering.

2.2. Fault Diagnosis Method Based on Order Analysis

2.2.1. Principle

Mechanical vibration is a powerful signal for directly reflecting the operation status of the equipment. The vibration of the gearbox during normal operation mainly comes from the meshing transmission of the gear. According to the difference of medium, it can be divided into air acoustic vibration and structural acoustic vibration. The structural acoustic vibration will be transmitted to the box along the shaft, bearing and other parts, which will be collected by the sensor. It can been seen in Figure 2, the signal acquisition system included pulse collector, vibration sensor (including signal amplifier and extension cable), signal acquisition and processing unit, and PC. In addition, PC had built-in special signal analysis and processing software. The vibration sensor was installed at the lifting of the loading and unloading hook in the right box of the gearbox, and its center line was perpendicular to the axis of the transmission shaft of the gearbox. If the direction of the transmission axis was Z, the actual vibration measurement was X and Y axis directions.

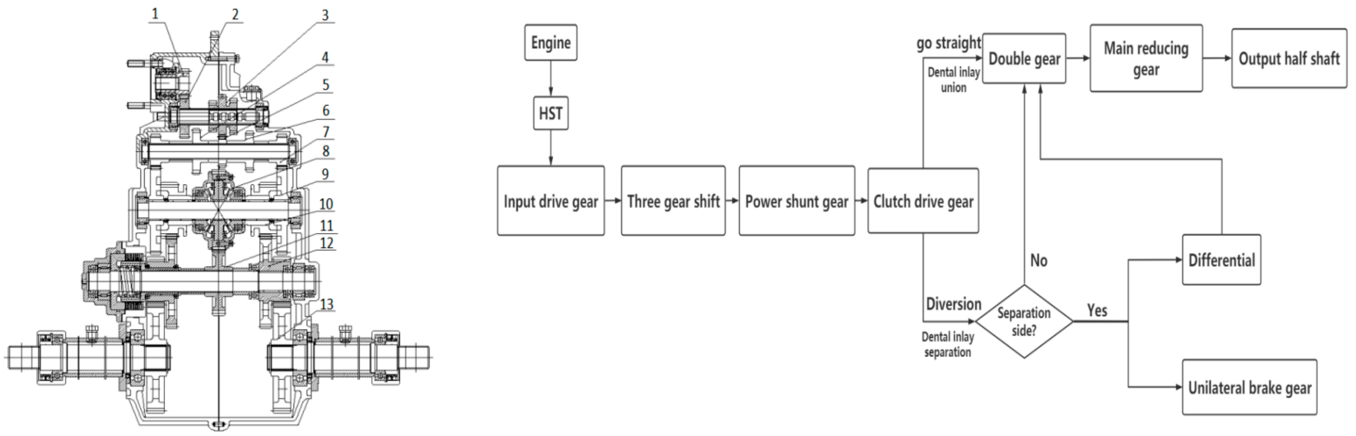

(**a**) Structure. (**b**) Simplified kinematic scheme.

Figure 1. Diagram of differential inverse gearbox: 1—Input driving gear; 2—Input driven gear; 3—Shift transmission gear (first gear, third gear, second gear from left to right); 4—First driven gear; 5—Third driven gear; 6—Second driven gear; 7—Power shunt gear; 8—Clutch driving gear; 9—Clutch driven gear; 10—Clutch driven gear; 11—Differential steering brake gear; 12—Double gear; 13—Main reducing gear.

Figure 2. Signal acquisition system.

The fault diagnosis method based on order analysis first converts a non-stationary vibration signal in the time domain into a stationary vibration signal in the angle domain. Then, the order spectrum, which clearly reflects each characteristic order, is obtained by fast Fourier transform (FFT). By comparing the peak changes in the spectral lines before and after looking up the order calculation table, the fault location and the corresponding fault type can be found. In this paper, the computational order analysis method (COT) based on spline interpolation was used to realize the equal angle sampling of vibration signals. The specific troubleshooting process is shown in Figure 3.

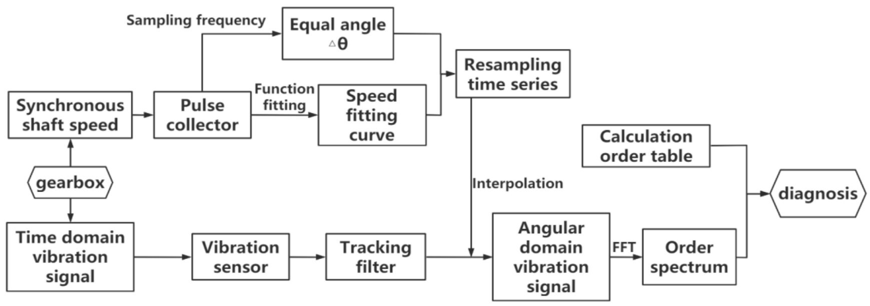

Figure 3. Fault diagnosis flow chart.

2.2.2. Order Calculation of Differential Inverse Gearbox

The relationship between frequency and order in rotating machinery structure is shown in Equation (1):

$$O = \frac{f}{f_1} \tag{1}$$

where O is the order, f is the frequency, and f_1 is the synchronous frequency.

In addition to rotating shafts, gears, and other structural components, there were a wide variety of bearings that support rotation in the gearbox. The rolling bearing was mainly composed of outer ring, inner ring, rolling body, and cage. The corresponding calculation methods are shown in Equations (2)–(5), respectively:

$$O_{oo} = |(C_o - O_o) \times n_b| \tag{2}$$

$$O_{oi} = |(C_o - O_i) \times n_b| \tag{3}$$

$$O_b = \left(\frac{d_{pc}}{d_b}\right) \times \left(1 - \left(\frac{d_b}{d_{pc} \times \beta}\right)^2\right) \times (|O_i - O_o|) \tag{4}$$

$$C_o = \frac{O_i}{2} \times \left(\frac{1 - (\cos b \times R_b)}{R_i + R_b}\right) + \frac{O_o}{2} \times \left(\frac{1 - (\cos b \times R_b)}{R_i + R_b}\right) \tag{5}$$

where O_{oo} is the outer ring order; O_{oi} is the inner ring order; O_b is the rolling body order; C_o is the cage order; O_i is the inner ring rotation order; O_o is the outer ring rotation order; b is the radian pressure angle; R_b is the rolling body radius; R_i is the inner ring radius; n_b is the number of rolling bodies; d_{pc} is the bearing pitch diameter; d_b is the roller diameter; β is the contact angle, β = cos $\alpha \times 3.14/\pi$; α is the pressure angle.

Because the torque speed sensor was installed on the output shaft at both ends of the differential steering gearbox, the output speed was taken as the synchronization object in the order calculation. The input data of differential inverse gearbox, the order calculation model of differential inverse gearbox and its main order are shown in Tables 1 and 2 and Figure 4, respectively. The first harmonic of key bearing order under medium speed gear is shown in Table 3.

Table 1. Input data of differential inverse gearbox.

Gear	Speed (R/min)	Torque (N.m)	Transmission Ratio	Power (kW)
First	2787	167	30.966	48.74
Second	2798	195	21.5	57.14
Third	2865	242	14.955	72.62

Table 2. Main order of differential steering gearbox in each gear.

Item	First Harmonic	Second Harmonic	Third Harmonic
First gear meshing	282.733	565.467	848.2
First gear input shaft	18.859	37.698	56.547
First gear output shaft	11.781	23.561	35.342
Second gear meshing	235.611	471.222	706.833
Second gear input shaft	13.089	26.179	39.269
Second gear output shaft	11.781	23.561	35.342
Third gear meshing	200.269	400.539	600.808
Third gear input gear	9.103	18.206	27.309
Third gear Output gear	11.781	23.561	35.342

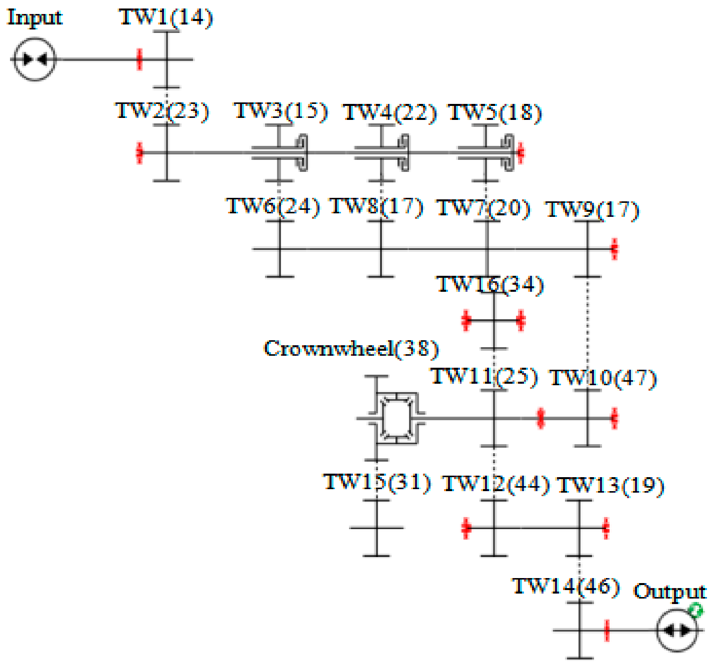

Figure 4. Order calculation model. The red dots are bearings.

Table 3. Main order of differential steering gearbox in each gear.

Model	Retainer	Inner Race	Outer Race	Rolling Element
6007RZ	9.3220	255.8257	195.7623	79.4098
NJ205E	5.3520	123.7995	85.6323	34.7195
6205E	4.8168	111.4199	77.0691	31.2476
NJ306E	1.6912	35.9776	23.6772	9.8933
51208	1.2105	18.1579	18.1579	6.5066
NJ2207E	1.0031	21.2697	15.0461	6.8562
6310	0.4118	8.8235	6.1765	2.7451

2.3. Durability Test

2.3.1. Gearbox Assembly Fatigue Test Bench

As shown in Figure 5, the durability fatigue test-bed for the gearbox assembly was composed of a main power cabinet, central control cabinet, driving device, loading device, small hydraulic station, torque speed sensor, sliding bearing seat, universal coupling, base and cushion, etc. When working, the main power supply cabinet started the drive motor, and the power was transferred to the input of the differential inverse gearbox through a five-slot B belt to drive the box to run. The tester could complete the test load spectrum loading, hydraulic steering control, and key test parameter monitoring on the central control cabinet.

The program control interface of the loading device is shown in Figure 6, which was compiled using the virtual instrument software Labview. The load was mainly composed of constant torque, alternating torque and noise. The alternating torque included sine wave, triangular wave, serration wave, square wave. At the same time, it had the functions of setting the test running time and real-time acquisition and displaying and storing test parameters such as torque and rotational speed.

2.3.2. Test Design

According to the actual field working conditions and gear frequency of the combine harvester, the fatigue test scheme was mainly divided into the following working conditions: small load forward (first gear, second gear, third gear), full load forward (first gear, second gear, third gear), unilateral brake left turn (first gear), unilateral brake right turn (first gear), differential left turn (first gear, second gear), differential right turn (first gear, second gear). The second gear was the common working gear of the differential inverse gearbox. Therefore, the running time ratio of the first gear, the second gear and the third gear was 1:2:1. Consult the relevant data [14], the time proportions of the operating conditions for small load forward, full load forward and left turn are 0.08, 0.75 and 0.08, respectively. The experiment is conducted for 12 h a day, and the specific shift schedule is shown in Table 4.

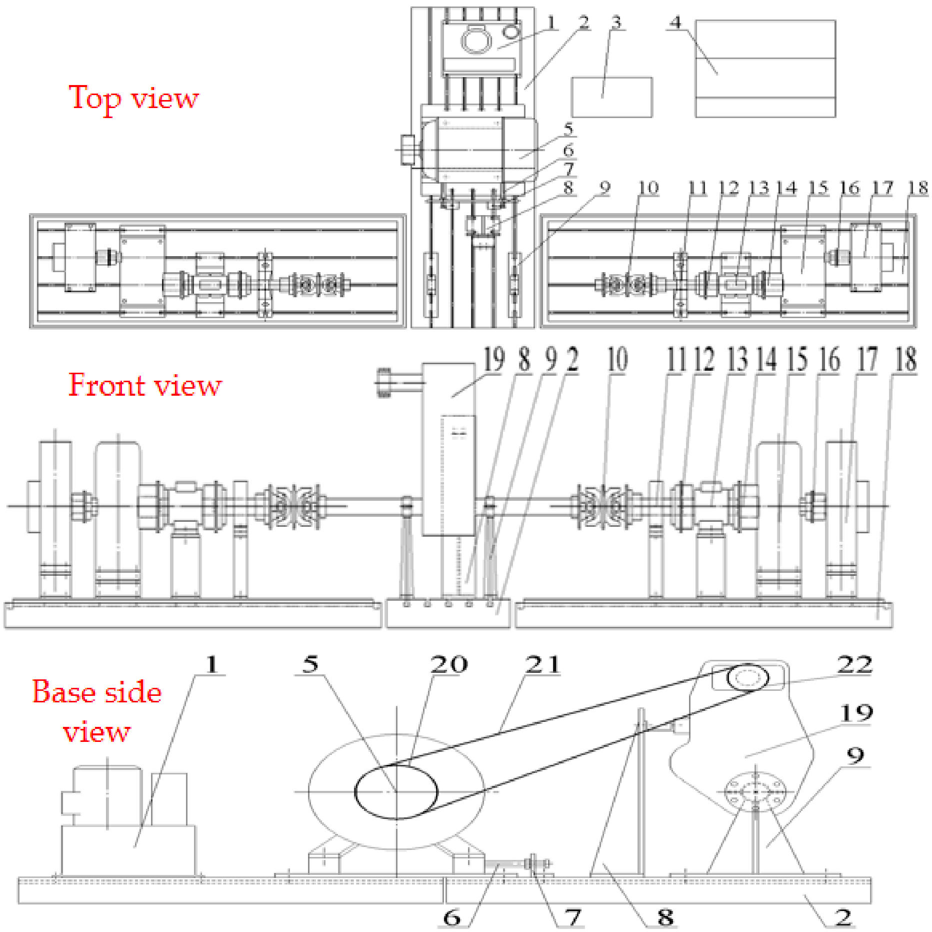

(**a**)

(**b**)

Figure 5. Gearbox assembly test bench structural schematic diagram (**a**) and physical diagram (**b**). 1. hydraulic station, 2. longitudinal installation base, 3. main power cabinet, 4. central control cabinet, 5. drive motor, 6. positioning bolt, 7. positioning support, 8. gearbox installation support, 9. gearbox fixed support, 10. universal coupling, 11. sliding bearing, 12. double coupling A, 13. torque speed sensor, 14. coupling B, 15. reduction box, 16. coupling C, 17. magnetic powder brake 18. transverse mounting support, 19. gearbox under test, 20. large pulley 21. five-slot B belt, 22. small pulley.

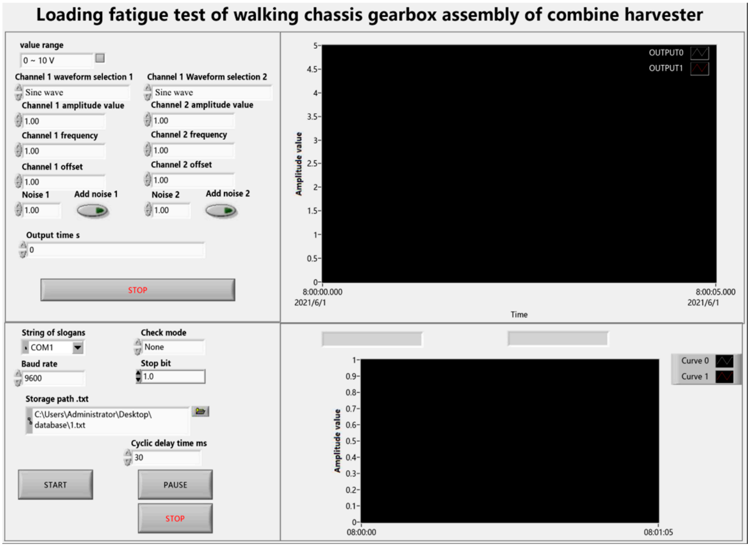

Figure 6. Program control interface.

Table 4. Schedule of shifts.

Shift	Gear	Time
First shift	First gear	8:00–9:00
	Second gear	9:00–11:00
	Third gear	11:00–12:00
Second shift	First gear	13:00–14:00
	Second gear	14:00–16:00
	Third gear	16:00–17:00
Third shift	First gear	18:00–19:00
	Second gear	19:00–21:00
	Third gear	21:00–22:00

The load spectrum data needed for the test were mainly from the research results [15–17]. According to the basic performance parameters of the combine harvester equipped with the differential steering gearbox, the whole machine weight was 3.64 t, the forward speed was 0–1.5 m/s, and the crop feed rate was 5 kg/s. The specific load values are shown in Tables 5 and 6.

Table 5. Proportion of working time under different working condition.

Gear	Left Half Shaft		Right Half Shaft	
	Small Load/kW	Full Load/kW	Small Load/kW	Full Load/kW
First gear	0.97	1.47	1.14	1.95
Second gear	2.35	6.62	2.76	8.34
Third gear	3.61	10.22	4.85	14.61

Table 6. Peak power of two steering modes in first gear and second gear.

Gear	Unilateral Brake Steering		Differential Steering	
	Left/kW	Right/kW	Left/kW	Right/kW
First gear	8.05	9.39	6.12	6.12
Second gear	9.68	11.27	10.98	10.98

To decrease the test cost, the relevant theory of accelerated fatigue test was used to strengthen the load data to get the load spectrum. The theoretical basis of accelerated fatigue test came from Miner's linear cumulative damage theory. Under the action of cyclic load, the fatigue damage of mechanical structure can be linearly accumulated, and the stresses were independent and irrelevant. Fatigue failure will occur when the cumulative damage reached a certain value. Common accelerated fatigue test methods included increasing test loading frequency, linear enhanced load spectrum method, nonlinear enhanced load spectrum method. The linear enhanced load spectrum method was to multiply the load amplitudes under different frequencies in the original load spectrum by an enhancement coefficient, while the frequency ratio corresponding to each load remains unchanged. The acceleration effect of the linear enhanced load spectrum on the fatigue test was remarkable. When the strengthening coefficient was small (close to 1), the enhanced load spectrum and the original load spectrum can well meet the similar load conditions of the Miner principle to ensure that the fatigue test results were consistent with the actual fatigue damage. Therefore, in this experiment, the load spectrum was enhanced by increasing the test loading frequency and linear strengthening load spectrum. The strengthened load data is shown in Table 7.

Table 7. Peak power of two steering modes in first gear and second gear: the forward working condition is uniformly used to carry a larger load of the right walking half shaft; the steering condition is unilateral braking steering in (), and the rest is differential steering; the time column takes the first shift time as an example, which is divided according to the running time of each gear.

Working Condition		Original Power/kW	Strengthening Power/kW	Strengthening Coefficient	Time/min
First gear	Small load	2.28	3.19	1.4	5
	Full load	3.9	4.68	1.2	50
	Left turn	6.12 (8.05)	8.57 (11.27)	1.4	5
	Right turn	6.12 (9.39)	8.57 (13.15)	1.4	5
Second gear	Small load	5.52	7.73	1.4	10
	Full load	16.68	20.02	1.2	100
	Left turn	10.98	15.37	1.4	10
	Right turn	10.98	15.37	1.4	10
Third gear	Small load	9.7	13.58	1.4	5
	Full load	29.22	35.06	1.2	50

According to the relevant data [18], the load change frequency of combine harvester under field conditions was generally within 2 Hz. Considering the limitation of response time of magnetic powder brake, the frequency range of alternating torque that can be set in the program control interface was 0–2 Hz, the fluctuation amplitude of alternating torque was 0–20% of constant torque, and the wave momentum range was 20 Nm. After completing the setting of the above parameters and running time, the automatic control of the loading device can be realized. The specific torque loading form is shown in Table 8.

Table 8. Torque loading form.

Working Condition		Constant Torque/Nm	Alternating Torque		Wave Momentum/Nm
			Amplitude/Nm	Frequency/Hz	
First gear	Small load	140	30	2	20
	Full load	210	40	2	20
	Left turn	540 (990)	110 (200)	2	20
	Right turn	540 (1150)	110 (250)	2	20
Second gear	Small load	240	50	2	20
	Full load	610	120	2	20
	Left turn	470	90	2	20
	Right turn	470	90	2	20
Third gear	Small load	300	60	2	20
	Full load	780	150	2	20

3. Results and Discussion

The start time of the test is 26 June 2021, and the whole test process was monitored by the fault diagnosis system. After a total of about 50 h of running time, the trend index curve suddenly rose and exceeded the alarm limit, and the alarm signal was issued at 15:45 on 4 July. The gearbox was in the small load of third gear condition.

3.1. Overall overview of trend curve

To clearly analyze the fault type and evolution process in the differential steering gearbox during the fatigue test, the global overview diagram of the trend index of each working condition was observed through the signal analysis and processing software of the fault diagnosis system, as shown in Figures 7–9. The trend index is the set of vibration energy amplitudes corresponding to all order points, and each trend index point is obtained by superposition and summation of change spectral lines. The calculation equation is shown in Equation (6). The limit value of the trend index depends on the comprehensive fatigue performance of the gearbox, which was determined as 3000 g through a large number of tests.

$$TI = \sum_{i=1}^{n} |X_i - Y_i| \tag{6}$$

where TI is the trend index, g; X_i is the actual energy amplitude corresponding to each sampling order, g; and Y_i is the upper and lower tolerance band limit obtained in the learning phase, g.

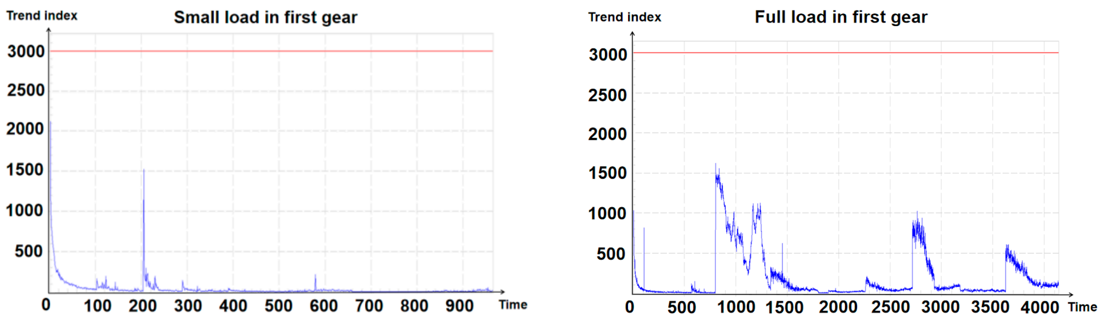

(**a**) (**b**)

Figure 7. Small load (**a**) and full load (**b**) in first gear.

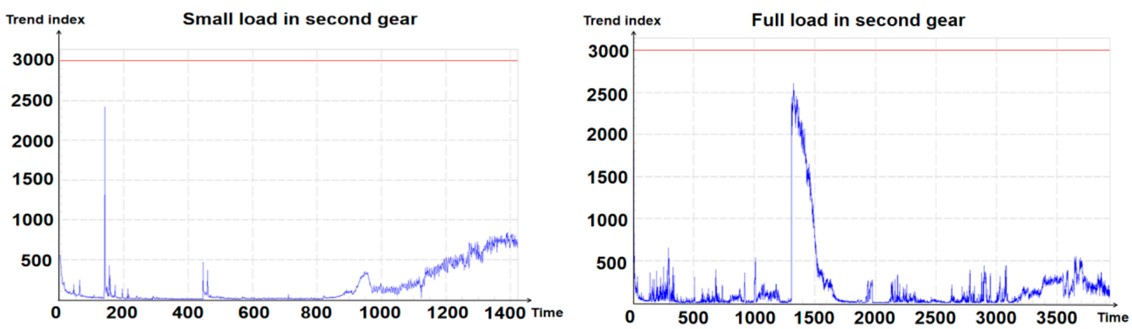

(**a**) (**b**)

Figure 8. Small load (**a**) and full load (**b**) in second gear.

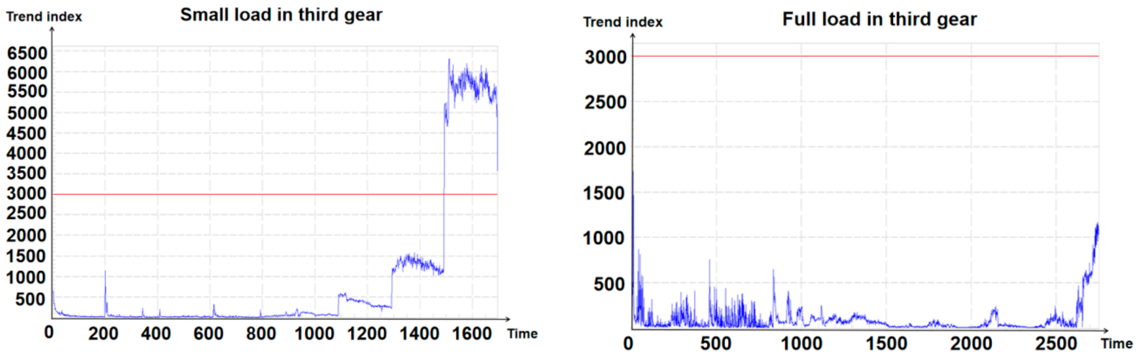

(**a**) (**b**)

Figure 9. Small load (**a**) and full load (**b**) in third gear.

Seeing Figures 7–9, the trend index curve of the fault diagnosis system exceeded the alarm limit under small load of third gear conditions, and the curve increased suddenly in many places at the same time. The trend curve increased obviously in the second gear low load condition, the second gear full load condition and the third gear full load condition. The sudden rise and slow decline of the trend index curve for a full load may be related to the change of oil temperature in the gearbox. By analyzing the boundary conditions of the six data cards, the test conditions such as torque and rotational speed were stable and all within the learning range. Therefore, the increase of the trend index curve was not caused by the test conditions, which indicated that the internal mechanical structure of the gearbox had changed.

Because the first gear trend curve was basically stable and the monitoring stage was greatly affected by the oil temperature, the fault analysis was only carried out for the second and third gear working conditions.

3.2. Third Gear Fault Analysis

Seeing Figure 10, according to the order calculation table of the differential steering gearbox, the order 200.25 in the figure was the meshing order of the third-gear master–slave gear, the meshing order of the power shunt gear and the tooth-embedded driving gear. The 167.5 order and 232.75 order in the diagram were the side frequencies of the meshing order, and the side frequency interval was 32.5, which was close to the third harmonic (35.342) of the shaft where the third-gear driven gear and power shunt gear were located. Therefore, the fault may occur on these two gears. Simultaneously, the order of the side frequency band was less, the distribution was more concentrated and the amplitude was higher, which was the typical characteristic of distributed fault pitting fatigue failure.

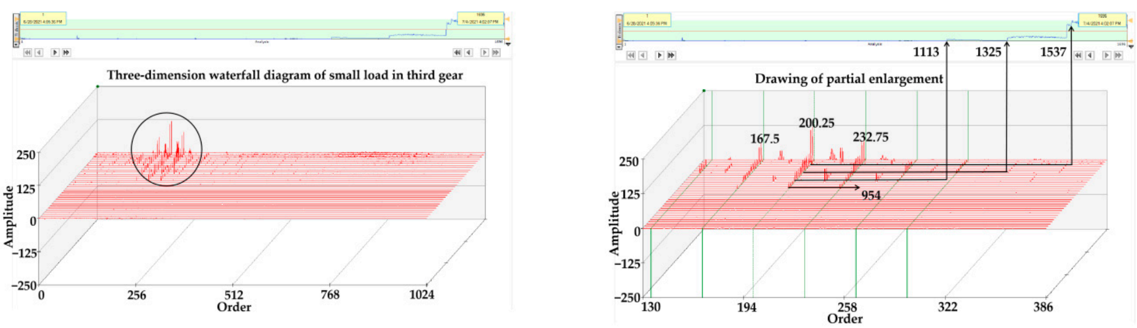

(**a**) (**b**)

Figure 10. Three-dimension waterfall diagram (**a**) and drawing of partial enlargement (**b**) of difference spectrum of small load in third gear.

It can be also seen from the Figure 10 that the fault first occurred in the 954th analysis, and the vibration amplitudes of the meshing order and side frequency began to increase at the 1113th and the 1325th analysis, respectively. This indicated that the fault was gradually intensifying. At the 1537th analysis, the energy amplitude reached the alarm limit and the shutdown was triggered, indicating that the fault had deteriorated to a certain extent. At the 135th analysis, there was a side frequency with an interval of 18.75 around the main meshing order, which was basically consistent with the second harmonic (18.2063) of the shaft frequency of the third-gear drive gear. According to the characteristics of less and concentrated side frequency, it was judged that the pitting corrosion phenomenon also occurred in the third-gear drive gear at this time. After unpacking, the damage of the gear inside the gearbox was consistent with the fault analysis results, as shown in Figure 11.

(**a**) (**b**) (**c**)

Figure 11. Damage of third-gear drive gear (**a**), third-gear driven gear (**b**) and power shunt gear (**c**) inside the gearbox.

Seeing Figure 12, in the 2717th analysis of the trend index curve under the third gear full load condition, the energy of the high-frequency part increased significantly, which may be attributed to metal friction in the gearbox body. This was completely consistent with the time of partial increase of high frequency energy during the 135th analysis under low load conditions, which began during the third-gear test from 21:00 to 22:00 in the evening of 3 July 2021. According to the unpacking results, high frequency metal frictions were occured on the side of the power shunt gear, the outer ring of the NJ205E cylindrical roller bearing and the wall of the housing hole of the box bearing, as shown in Figure 13.

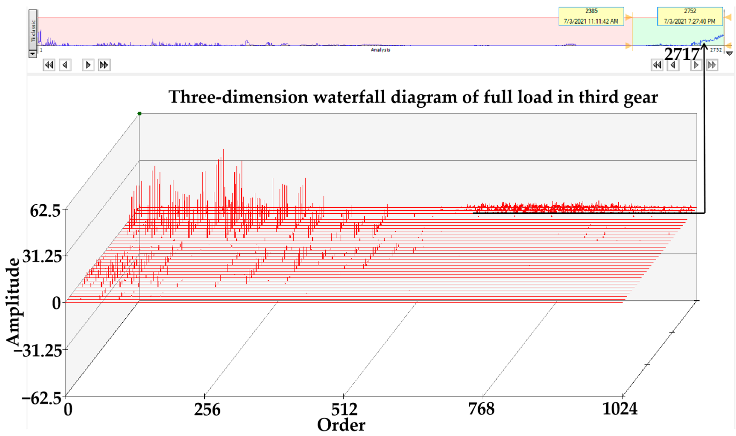

Figure 12. Three-dimension waterfall diagram of full load in third gear.

(**a**) (**b**) (**c**)

Figure 13. Internal damages of power shunt gear side (**a**), NJ205E cylinder roller bearing (**b**) and bearing hole wall (**c**).

3.3. Second Gear Fault Analysis

As shown in Figure 14, with the small increase in the energy of the low-frequency part in varying degrees, the trend index curve indicating the change of mechanical vibration characteristics in the gearbox began to rise slowly. This indicated that there was some kind of fault in the internal mechanical structure of the gearbox. A side frequency band with an interval of 45 appeared around the 235th order, which was exactly the same as the fourth harmonic of the shaft frequency of the second driven gear. According to the characteristic that the band order of this side was small and concentrated, it was judged that the pitting distributed fault may occur in the second driven gear. This fault can also be observed in the 3D waterfall diagram of the second gear full load, as shown in Figure 15, and the fault occurred at the same time. The gear damage after unpacking can be seen in Figure 16. This was basically consistent with the results of fault analysis.

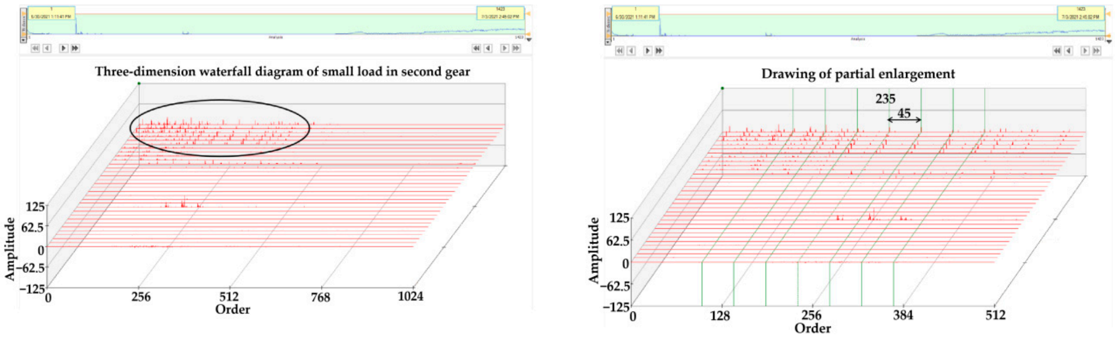

(**a**) (**b**)

Figure 14. Three-dimension waterfall diagram (**a**) and drawing of partial enlargement (**b**) of difference spectrum of small load in second gear.

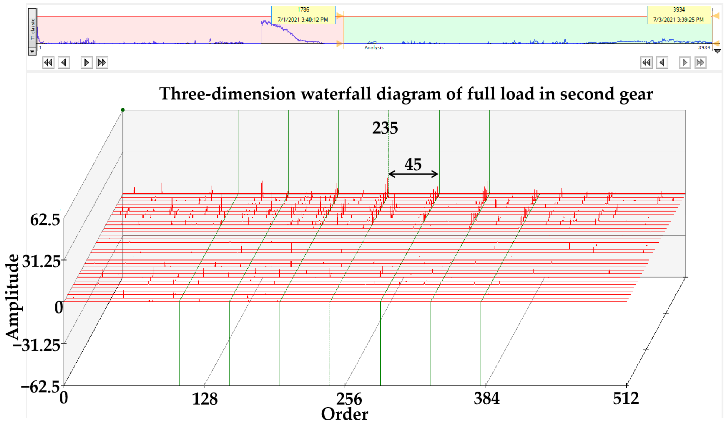

Figure 15. Three-dimension waterfall diagram of full load in second gear.

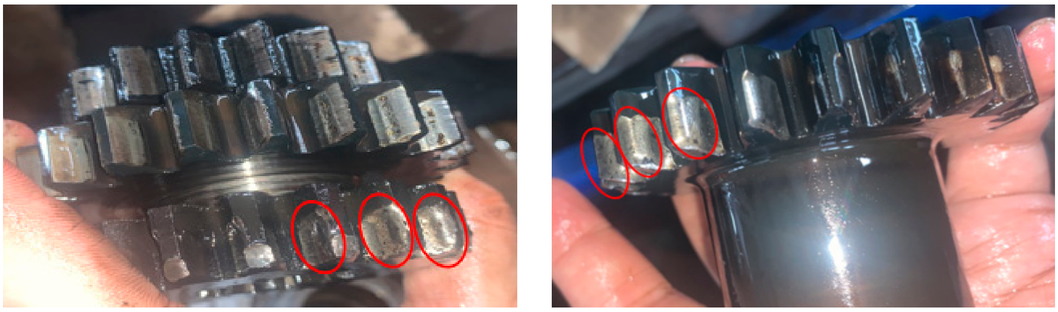

(**a**) (**b**)

Figure 16. Damage of second drive gear (**a**) and second driven gear (**b**) inside the gearbox.

4. Conclusions

A fault diagnosis method for a differential inverse gearbox of a crawler combine harvester based on order analysis was studied in this paper. The main conclusions were as follows:

- The edge frequencies with an interval of 45 with few edge band orders and relatively concentrated distribution appeared around meshing order 235 of the second-gear master–slave gear, and the edge frequency with an interval of 32.5 and 18.5 with few edge band orders and relatively concentrated distribution appeared around the meshing order 200.25 of third-gear master–slave gear, power shunt gear and clutch driving gear. This indicated that pitting distributed faults occurred in the second-gear driven gear, third-gear master–slave gear and power shunt gear. This was consistent with unpacking and inspection.
- This method can send out the test stop signal according to the vibration energy level of the test object and can reflect the possible early fault type and location to the test personnel through the order spectrum generated under each gear without unpacking the gearbox. This had reference significance for research on the fault diagnosis method of a crawler combined harvester gearbox.

Author Contributions: Data curation, Y.L. (Yanbin Liu) and R.Z.; Funding acquisition, Y.L. (Yaoming Li); Investigation, R.Z.; Methodology, Y.L. (Yanbin Liu) and R.Z.; Project administration, Y.L. (Yaoming Li); Supervision, K.J.; Validation, R.Z.; Writing—Original draft, Y.L. (Yanbin Liu); Writing—Review & editing, K.J. All authors have read and agreed to the published version of the manuscript.

Funding: The work was supported by Jiangsu Province's major scientific and technological achievements Transformation project (BA2020054), Major scientific and technological innovation project in Shandong Province (2019jzzy010729).

Institutional Review Board Statement: Not applicable.

Informed Consent Statement: Not applicable.

Data Availability Statement: Not applicable.

Conflicts of Interest: The authors declare no conflict of interest.

References

1. Li, Y.; Tian, J.; Zhao, Z.; Xu, L. Fatigue analysis of gears in combine harvester chassis gearbox. *Trans. Chin. Soc. Agric. Eng.* **2011**, *27*, 106–110.
2. Li, B.; Tang, B.; Deng, L.; Wei, J. Joint attention feature transfer network for gearbox fault diagnosis with imbalanced data. *Mech. Syst. Signal Process.* **2022**, *176*, 109146. [CrossRef]
3. Su, Y.; Meng, L.; Kong, X.; Xu, T.; Lan, X.; Li, Y. Small sample fault diagnosis method for wind turbine gearbox based on optimized generative adversarial networks. *Eng. Fail. Anal.* **2022**, *140*, 106573. [CrossRef]
4. Ha, J.M.; Youn, B.D. Fault diagnosis of a planetary gearbox by D norm-based time synchronous averaging (DTSA) with roughly estimated phase information under an encoder-less operating condition. *J. Sound Vib.* **2022**, *520*, 116545. [CrossRef]
5. Yuan, X.; Cai, L. Variable amplitude Fourier series with its application in gearbox diagnosis-Part II: Experiment and application. *Mech. Syst. Signal Process.* **2005**, *19*, 1067–1081. [CrossRef]
6. Li, B. *Research on the Generalized Demodulation Time-Frequency Analysis Method and Application to Gear Fault Diagnosis*; Hunan University: Changsha, China, 2010.
7. Feng, Z.; Chen, X.; Wang, T. Time-varying demodulation analysis for rolling bearing fault diagnosis under variable speed conditions. *J. Sound Vib.* **2017**, *400*, 71–85. [CrossRef]
8. Lin, J.; Zhao, M. Dynamic signal analysis for speed-varying machinery: A review. *Sci. Sin.* **2015**, *45*, 669–686.
9. Feng, Z.; Chen, X.; Liang, M. Joint envelope and frequency order spectrum analysis based on iterative generalized demodulation for planetary gearbox fault diagnosis under nonstationary conditions. *Mech. Syst. Signal Process.* **2016**, *76–77*, 242–264. [CrossRef]
10. Wan, D.; Sun, D.; Zhao, Y. Synchronous revolution order analysis application in fault diagnosis of auto gearbox. *Comput. Meas. Control* **2006**, *3*, 299–300.
11. He, G.; Ding, K.; Li, W.; Jiao, X. A novel order tracking method for wind turbine planetary gearbox vibration analysis based on discrete spectrum correction technique. *Renew. Energy* **2016**, *87*, 364–375. [CrossRef]
12. Chen, J. *Dynamic Analysis and Experimental Study for the Differential Steering System of the Tracked Combine Harvester*; Jiangsu University: Zhenjiang, China, 2016.
13. Huang, J. *Design and Experimental Study on Differential Inverse Gearbox of Tracked Rice Field Combine Harvester*; Jiangsu University: Zhenjiang, China, 2018.
14. Ye, X.; Li, Y.; Xu, L.; Pang, J.; Ma, Z. Fatigue analysis half axle of combine harvester. *J. Agric. Mech. Res.* **2014**, *36*, 32–35.
15. Li, Y.; Ye, X.; Xu, L.; Pang, J.; Ma, Z. Construction and performance experiment of load test system for half axle of combine harvester. *Trans. Chin. Soc. Agric. Eng.* **2013**, *29*, 35–41.
16. Li, Y.; Chen, J.; Liang, Z.; Ma, X.; Jiang, X. Design and experiment of differential steering mechanism for track combine harvester. *Trans. Chin. Soc. Agric. Mach.* **2016**, *47*, 127–134.
17. Ji, X.; Li, Y.; Xu, L.; Pang, J.; Ye, X. The design and experiment of load measurement system for combine harvester. *J. Agric. Mech. Res.* **2013**, *35*, 131–134.
18. Ye, X. *Load Testing and Reliability Analysis of Combine Harvester Halt Axle*; Jiangsu University: Zhenjiang, China, 2013.